DOSIMETRIC CHARACTERIZATION OF ELONGATED BRACHYTHERAPY SOURCES USING MONTE CARLO METHODS

A Thesis
Presented to
The Academic Faculty

by

Elizabeth Bannon

In Partial Fulfillment
of the Requirements for the Degree
Masters in Medical Physics in the
School of George W. Woodruff School of Mechanical Engineering

Georgia Institute of Technology
April 2010

DOSIMETRIC CHARACTERIZATION OF ELONGATED BRACHYTHERAPY SOURCES USING MONTE CARLO METHODS

Approved by:

Mark J. Rivard, Ph.D. Advisor
Tufts Medical Center
Tufts University

C.-K. Chris Wang, Ph.D.
George W. Woodruff School of Mechanical Engineering
Georgia Institute of Technology

Sang Hyun Cho, Ph.D.
George W. Woodruff School of Mechanical Engineering
Georgia Institute of Technology

Date Approved: March 17, 2010

For Huckleberry and the Nugget

ACKNOWLEDGEMENTS

I would like to thank my advisors, both Dr. Mark Rivard at Tufts Medical Center and Dr. Chris Wang at Georgia Institute of Technology, for their advice, opinions and willingness to help me out of sticky situations. I would like the incredible group of people who work in Radiation Oncology at Tufts Medical Center for indulging my questions and eating my cake, particularly Dr. Chris Melhus and Mr. Martin Fraser. The knowledge I have gained while working with them is immeasurable. I must also thank the students in the distance learning Medical Physics program, particularly Kelly Mannella, Angie Rohrer, Donna Ghorbanpoor and Danny Harrington, who commiserated with, laughed with, studied with, complained with and encouraged me, and without whom I would never have succeeded. Finally, I especially wish to thank my husband, Brad, and my daughter, Leela, for giving me a reason to continually strive for new heights.

TABLE OF CONTENTS

LIST OF TABLES

LIST OF FIGURES

SUMMARY

Current brachytherapy treatment planning systems are unable to accurately calculate dose distributions in the vicinity of brachytherapy sources having active lengths much greater than 5 mm. While low dose-rate ^{137}Cs sources are dosimetrically characterized using antiquated along-away tables with simple linear-linear interpolation errors in dose calculation exceeding 30% occur due to algorithm inadequacy. The method presented in this thesis permits dosimetric characterization of elongated brachytherapy sources with active lengths $0 \leq L \leq 10$ cm for implementation on an FDA-approved clinical TPS. Low- and high-energy photon-emitting sources of ^{103}Pd and ^{192}Ir, respectively, were examined.

CHAPTER 1

INTRODUCTION

Radiation has been used for over a century as a method to combat the spread of cancer.[1,2] Soon after clinical application of external radiation sources, the idea of implanting radioactive sources into diseased tissue was considered.[3] This modality is known as brachytherapy and was first utilized prior to the First World War. Small seeds have been used as the radiation source for much of the recent history of brachytherapy. In the past decade, the technology used to make brachytherapy sources has developed to a point where threadlike structures are now readily available with high pliability and a uniform radioactivity distribution.

Arguably, the most important job of the medical physicist is accurately determining the dose a patient is going to receive during treatment. Much work has been accomplished by the radiotherapy community to improve the ability of medical physicists to predict the dose. For brachytherapy, this has meant modeling the dose distribution from a small source. At the outset of the modality, look up tables were used to estimate dose.[4,5,6] As technology became more complex, so did the algorithms; particularly when computers became commonplace. Currently, these algorithms superimpose precalculated source dose distributions over patient anatomy that is obtained using either CT or MRI data so that the dose estimation is determined for each individual patient implant. The American Association of Physicists in Medicine (AAPM) Task Group 43 (TG-43) established the global standard for brachytherapy dose calculation using these algorithms.[7,8,9]

The current approach for dose calculation relies on superposition of single-source dose distributions obtained in a liquid water phantom of a fixed volume for radiation scattering. The dose distribution is assumed to be cylindrically symmetrical. Dose from

each source is calculated and then the total dose from all sources is taken to be the sum of the individual sources.

This model works well for brachytherapy seeds with active lengths $L \leq 0.5$ cm; however, the medical community is considering the use of sources that cannot accurately be modeled as point sources.[10,11,12] Elongated sources, assumed to be substantially greater than 0.5 cm in length, have a different dose profile than conventional brachytherapy sources because of attenuation along the length of the source. Additionally, the point-source approximation breaks down at close distances from the source (*i.e.*, $r < L$), making it inadequate to consider the elongated source as merely the sum of a series of individual seeds. While a line source can be modeled using Monte Carlo methods for radiation transport simulations, this computational process is too resource intensive for most hospitals to be considered for individualized patient treatment planning in a clinical setting. The series of AAPM TG-43 reports (*i.e.*, Nath *et al*. 1995, Rivard *et al*. 2004, Rivard *et al*. 2007) mentioned above were developed specifically for seed-like sources and therefore has a few specific problems that need to be addressed in order for accurate dose calculations to be made within the treatment planning systems (TPS).

This thesis aimed to determine if an elongated source can be accurately modeled using smaller lengths. The goal was to develop a mathematical model that combined smaller sources in such a way that the dose distribution was sufficiently similar to the elongated brachytherapy source. Monte Carlo simulations were conducted to evaluate the dose distributions of various lengths of ^{103}Pd and ^{192}Ir. This work was performed in conjunction with the AAPM TG-143, which has the charge of developing a new dose calculation formalism and associated guidelines for clinical implementation of elongated brachytherapy sources of photon emitting radionuclides.

CHAPTER 2

BACKGROUND

Manufacturers produce radioactive sources in a variety of shapes, increasing the clinical possibilities for brachytherapy treatment. One particular shape that needs further investigation is a flexible threadlike source which may be cut to the desired length.

2.1 AAPM TG-43 Dosimetry Protocol for Interstitial Brachytherapy Sources

The AAPM TG-43U1 formalism is currently used in brachytherapy TPS to calculate clinical dose distributions.[8] The formalism has 1D and 2D formats: the point-source approximation and the line-source approximation. The latter formalism is generally used in this thesis, and is represented with the following equation:

$$\dot{D}(r,\theta) = S_K \Lambda \frac{G_L(r,\theta)}{G_L(r_0,\theta_0)} g_L(r) F(r,\theta) \qquad (\mathbf{1})$$

where r is the distance (cm) from the center of the active source to the point of interest, θ is the polar angle (degrees) to the point of interest, S_K is the air-kerma strength of the source (μGy m^2 h^{-1}), Λ is the dose-rate constant, $G_L(r,\theta)$ is the line-source geometry function, $g_L(r)$ is the line-source radial dose function, and $F(r,\theta)$ is the 2D anisotropy function. The subscript $_0$ refers to the reference point, which is taken to be $r_0 \equiv 1$ cm and $\theta_0 \equiv 90^\circ$ as shown in Figure 2-1.

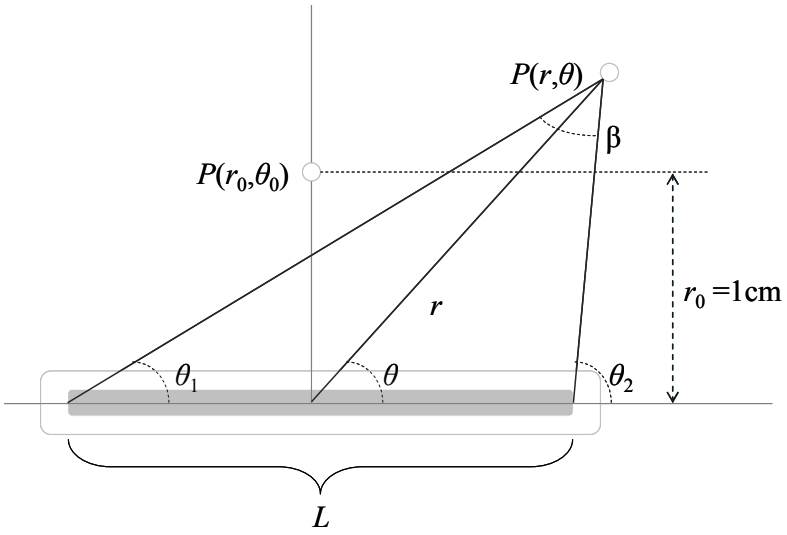

Figure 2-1 Coordinate system used for brachytherapy dosimetry calculations in TG-43U.

The dose-rate constant, Λ, is defined as the ratio of dose rate to water at the reference position in a water phantom divided by the source air-kerma strength.

$$\Lambda = \frac{\dot{D}(r,\theta)}{S_K} \tag{2}$$

The geometry function accounts for the spatial distribution of radioactivity within the source. For the purposes of this thesis, the source geometry is cylindrically-symmetric as is most always used in a clinical setting. $G_L(r,\theta)$ is defined as:

$$G_L(r,\theta) = \begin{cases} \dfrac{\beta}{Lr\sin\theta} & \text{if } \theta \neq 0^\circ \\ \left(\dfrac{r^2 - L^2}{4}\right)^{-1} & \text{if } \theta = 0^\circ \end{cases} \tag{3}$$

where β is the angle (radians) that is subtended by the ends of the hypothetical line source with respect to the point of calculation. (See Figure 2-1) $g_L(r)$ takes into account the effect of absorption and scatter along the transverse plane and is normalized to unity at r_0.

$$g_L(r) = \frac{\dot{D}(r,\theta_0)G_L(r_0,\theta_0)}{\dot{D}(r_0,\theta_0)G_L(r,\theta_0)} \quad (4)$$

$F(r,\theta)$ corrects for the change in dose as the polar angle changes for a fixed radius when dividing out the effect of the geometry function.

$$F(r,\theta) = \frac{\dot{D}(r,\theta)G_L(r,\theta_0)}{\dot{D}(r,\theta_0)G_L(r,\theta)} \quad (5)$$

2.2 Dose calculation models for elongated brachytherapy sources

Karaiskos' Method

The first of the methods that is being used for comparison was published by Karaiskos *et al*.[10,13] Limiting their calculations to source lengths between 3.0 cm and 7.0 cm, and using the TG-43 formalism, the parameters necessary to calculate dose are calculated in the following way.

1. Tables exist for $F(r,\theta)$ for 3.0 cm, 5.0 cm and 7.0 cm. Values of $F(r,\theta)$ are interpolated from these existing tables.
2. $g(r)$ is set equal to $g(r)$ for L = 5.0 cm.
3. $G_L(r,\theta)$ is calculated in the following manner:

$$G_L(r,\theta) = \left(\frac{L}{5.0\text{cm}}\right)^2 G_{5.0\text{cm}}(r,\theta) \quad (6)$$

4. Λ is calculated in the following manner:

$$\Lambda_L = \Lambda_{5.0\text{cm}} \frac{G_L(r_0,\theta_0)}{G_{5.0\text{cm}}(r_0,\theta_0)} \quad (7)$$

From these parameters, it is possible to calculate the dose using the TG-43 formalism.

The Karaiskos' Method has drawbacks in clinical implementation. First, the dose for L < 3.0 cm cannot be calculated using this method, which is not a reasonable condition to place upon clinical practice given the goal of developing a general dose calculation method for elongated brachytherapy sources. Second, it is not possible to

calculate dose for lengths that are curvilinear, a clear drawback in clinical situations as bending of the elongated source is most likely to occur after implantation. If a physician would like to place a source along the seam of a surgical cut, for example in a lung resectioning that would benefit from additional radiation treatment to improve the likelihood of cancer eradication, it becomes necessary to bend the source length to conform to the tumor bed. Third, this method cannot be used in a conventional brachytherapy TPS. In most brachytherapy TPS, $F(r,\theta)$ and $g(r)$ are the dosimetry parameters with values that are inputted by then clinical brachytherapy dose calculations are performed. The Karaiskos' Method deviates unacceptably from the AAPM TG-43 dose calculation method for this to be implemented in a conventional brachytherapy TPS. For example, Λ has a novel definition in the Karaiskos' Method, as does $G_L(r,\theta)$. Because there is no way to alter the methods used in the TPS to calculate the parameters, this method is rendered unusable clinically with current brachytherapy TPS.

Point-segmented source method (PSS)

Developed by Meigooni *et al*,[11] the PSS Method approximated a linear brachytherapy source by dividing it into 0.5 or 1.0 cm lengths and then treating each length as if it was a point source. In order to calculate a series of point sources, Meigooni *et al* used the AAPM TG-43 1D dose calculation formalism that is contained in the AAPM Task Group 43 Report, as defined by the following:

$$\dot{D}(r,\theta) = S_K \Lambda \frac{G_L(r,\theta_0)}{G_L(r_0,\theta_0)} g_L(r)\phi_{an}(r) \qquad (8)$$

This 1D formalism is similar to that of the 2D formalism. $F(r,\theta)$ has been replaced with a 1D anisotropy function, which Meigooni *et al* defined as

$$\phi_{an}(r) = \frac{\int_0^{90} \dot{D}(r,\theta)\sin\theta d\theta}{2\dot{D}(r,\theta_0)} \qquad (9)^{14}$$

The simulation was a straightforward approximation, where the extended source was broken up into segments, and the formalism was then applied. Two geometries were calculated: the first divided a 3.0 cm segment into six points spaced 0.5 cm apart while the second divided a 3.0 cm segment into three points spaced 1.0 cm apart. Once the point sources were positioned, the superposition principle was applied, summing the contribution from each point at every point in the grid location within the volume of interest.

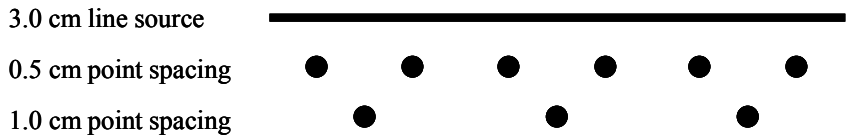

Figure 2-2 Point-segmented source method to approximate a 3.0 cm long brachytherapy source using spacing of 0.5 cm and 1.0 cm.

In order to account for radiation attenuation along the source long-axis, the point source parameters were calculated with dummy seeds in place as well, in addition to the simulations outlined above. The point source was placed in and amongst placement holders for source lengths in order to assure that proper attenuation conditions were met.

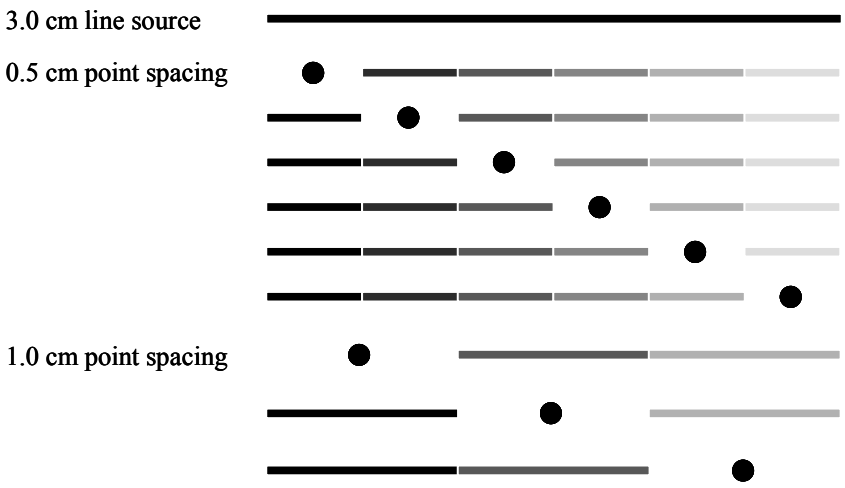

Figure 2-3 Attenuation correction for PSS. The circles represent the placement of point sources in the Monte Carlo simulations while the lines are dummy source lengths that were placed to account for attenuations conditions.

Monte Carlo simulations were calculated for the 3.0 cm RadioCoil™ using a dose grid of 0.5 cm spacing in the *z* (along the length of the source) and *y* (away from the source) directions. (See Figure 2-4) Additionally, in order to implement the PSS Method in the brachytherapy TPS, the parameters necessary to perform the dose calculations using the AAPM TG-43 formalism were calculated using Monte Carlo simulations as well. The parameters were inputted into brachytherapy TPS and the PSS Method was clinically implementable. This was an improvement over the Karaiskos' Method.

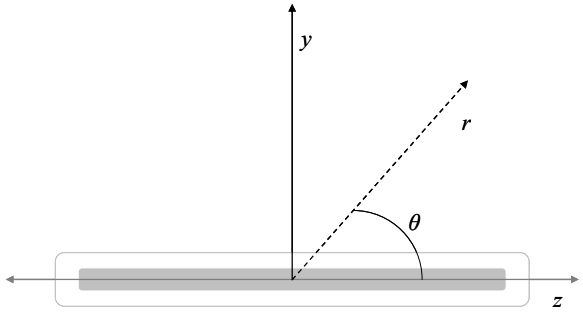

Figure 2-4 Coordinate system used for PSS, LSS, and TLS Methods

For points where $y \geq 1.0$ cm, the PSS Model under-approximated the Monte Carlo calculated dose by as much as 8% for the 0.5 cm spacing and by 12% for the 1.0 cm spacing. For $y < 1.0$ cm, these errors increased further. Differences as high as 34% at specific points were reported.

One concern with the PSS Method is the dose grid size used for the Meigooni *et al* Monte Carlo simulations. The calculation dose grid was 1.0 mm and volume averaging over the voxels smoothed out dose distributions in regions with higher gradients. Additionally, the PSS Method limitations in source length ($L < 3.0$ cm can not be modeled), which makes this method unusable in a clinical setting.

Line-segmented source (LSS) Method

The LSS Method is similar to the PSS Method, except instead of using point sources to model the active lengths of radioactivity, line segments were used, in 0.5 and 1.0 cm lengths. (See Figure 2-5 and Figure 2-6)

Figure 2-5 LSS approximation for a 3.0 cm length, using spacing of 0.5 cm and 1.0 cm.

The 2D formalism introduced in the AAPM TG-43U1 report was used in the LSS Method in order to perform calculations in the TPS. Monte Carlo simulations were performed to obtain the parameters necessary for TG-43 implementation in the TPS.

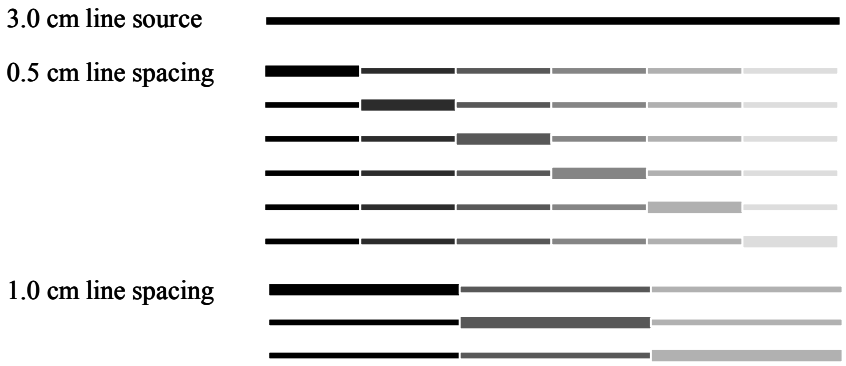

Figure 2-6 Attenuation correction for LSS. The thick lines are the sections that are radioactive. The thin lines represent dummy sources that were placed in the Monte Carlo simulations to account for attenuations.

For both simulations, meaning when the 3.0 cm source was divided into 6 segments or 3 segment, comparison of the Monte Carlo simulation and the dose calculations performed by the TPS using the LSS model (without source attenuation) showed 4% agreement when $\theta = 90°$, for values of r ranging from 0.5 cm to 2.0 cm. However, the differences were as high as 14%, which occurred at $\theta = 14°$ and $r = 2.06$ cm. When source attenuation was taken into account, differences increased even further to as much as 21%, again along the length of the source, just outside of the cap ($1.5 \text{ cm} < z < 2.5 \text{ cm}$).

Close distance approximation discrepancies were high enough to render this method unusable in clinical settings, as the AAPM usually demands a standard of care with accuracy of at most 3%. Additionally, the LSS Method suffers from many of the same problems as the PSS Method by not being implementable in the clinic and it cannot approximate lengths less than 3.0 cm with conventional brachytherapy TPS.

Two-line-source (TLS) Method

The TLS method to correct for dose anisotropy along the source length was developed by van der Laarse *et al.*[12] For $L > 1.5$ cm, the total length is divided into two

lengths: two peripheral lengths ranging between 0.75 cm and 1.25 cm, and a series of 1.0 cm inner lengths. For example, a 4.4 cm length would be divided into four segments: two outer segments of 1.2 cm each and two inner segments of 1.0 cm. To determine the various components for dose calculation, the following rules are used.

1. The geometry function is calculated according to the expression recommended by the AAPM TG-43U1 formalism for a line source:
   Λ is obtained in a way similar to that used by Karaiskos *et al*[10] by interpolating or extrapolating over the Λ values for 0.5 and 1.0 cm wires and correcting for the geometry by dividing out $G_L(r,\theta)$ for both lengths:
   $$\frac{\Lambda_L}{G_L(r_0,\theta_0)} = \frac{\Lambda_{0.5\,\mathrm{cm}}}{G_{0.5}(r_0,\theta_0)} + \left[\frac{\Lambda_{1.0\,\mathrm{cm}}}{G_1(r_0,\theta_0)} - \frac{\Lambda_{0.5\,\mathrm{cm}}}{G_{0.5}(r_0,\theta_0)}\right]\frac{L - 0.5\,\mathrm{cm}}{1.0\,\mathrm{cm} - 0.5\,\mathrm{cm}} \qquad (10)$$
2. If a wire length is smaller than 1.0 cm, $g_L(r)\mathrm{F}(r,\theta)$ are interpolated from tables containing data for $L = 0.5$ and $L = 1.0$ cm.
3. $g_{0.5\mathrm{cm}}(r) = g_{1.0\mathrm{cm}}(r)$, therefore $g_{1.0\mathrm{cm}}(r)$ is used for all lengths.

The TLS Method was a great improvement over the previously mentioned methods. Agreement with Monte Carlo simulations was 5.6% along the central axis of the source and some locations within the grid space had agreement within 2%. However, this method suffers from the same problem of an inability to readily apply it in a clinical setting. Λ has a novel definition in this study that differs from that which is used in the TPS, although this could be calculated offline as it is a scalar value. However, with the change in definition of $g_L(r)$ and $F(r,\theta)$, and the complexity of the calculations in the TLS Method, this would become a non-trivial problem that would need to be overcome for clinical use. Therefore, the TLS Method is rendered unusable outside of theoretical uses within the bounds of research.

2.3 Areas for improvement and rationale for research

As has been previously stated, the methods described in the literature suffer from a myriad of problems, the most pressing one being a lack of implementability within the current TPS models for brachytherapy calculations. In order for a method to be considered useful clinically, it needs to solve for $g_L(r)$ and $F(r,\theta)$ while using the standard definition for the geometry function. Additionally, the method needs to be usable for any length that may possibly be used clinically, which is technically only limited to the lengths that are produced by the vendors.

In this work, we take the first steps in the development of a method that will divide lengths into smaller segments that are more manageable. Using Monte Carlo simulations for various lengths of straight wire, we determined $g_L(r)$ *and* $F(r,\theta)$ using the Tufts technique developed by Rivard *et al*.[15] Unlike previous methods, this technique does not redefine any of the parameters that are laid out by TG-43U, which ensures that the method may be implemented within a conventional brachytherapy TPS. Once $g_L(r)$ and $F(r,\theta)$ are calculated for each length, this data was inputted into the Pinnacle TPS (v 8.0m, Phillips Medical Systems, Cleveland, OH). Using the Pinnacle TPS, a variety of lengths were compared to test the efficacy of the method. This testing was performed with the IBA Dosimetry OmniPro I'mRT radiation dosimetry software (v.1.6, $iba_{Dosimetry}$, Schwarzenbruck, Germany).

CHAPTER 3

METHODS

3.1 Overview

In order to ensure the ability to use our method within the TPS, data necessary for input was identified. As the method implemented by the TPS was based on the updated AAPM TG-43 formalism, we used that as our guiding principle. For calculating the dose, it is necessary to provide the TPS with $g_L(r)$, $F(r,\theta)$ and Λ. These values are length dependent, so it becomes necessary to input these functions for each length that is intended to be used in the TPS.

It was decided that we would model both a 3.0 cm length and 5.0 cm length using various smaller lengths and compare that data to Monte Carlo simulations. These lengths were chosen for comparison to Meigooni *et al*.[11] (3.0 cm) and van der Laarse *et al*.[12] (5.0 cm). To that end, Monte Carlo simulations were performed for a variety of lengths for both radionuclides and each Monte Carlo simulation was then used to calculate $g_L(r)$ and $F(r,\theta)$ for each length. These values were inputted into the TPS, and the TPS was used to "build" longer brachytherapy sources from various smaller lengths.

3.2 Geometry of wires

Two types of brachytherapy wires (^{103}Pd and ^{192}Ir) were modeled.

Palladium

The ^{103}Pd RadioCoil™ geometry was used in order to ensure that results were comparable to previously published work by the Meigooni team. RadioCoil™ sources are a flat ribbon of cyclotron-activated ^{102}Rh (ρ = 12.45 g/cm^3), which produces radioactive ^{103}Pd uniformly distributed throughout by the ^{102}Rh(p,n)^{103}Pd reaction. This metal is then

coiled into a 0.8 mm outer diameter ribbon with a hollow core, with lengths ranging from 1.0 cm to 6.0 cm at 1.0 cm increments. The core was taken to be water (ρ = 0.998 g/cm^3) instead of air. This was justified by running a Monte Carlo simulation with an air core and comparing it to the same length with a water core. The ratio of the results from a water core to those of an air core averaged 1.0061 along the transverse plane and 1.0070 throughout the space. One 3.0 cm length Monte Carlo simulation was completed with a core of air to ensure that the results with a water core were accurate. See Figure 3-1.

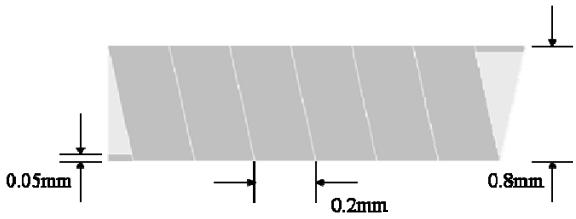

Figure 3-1 ^{103}Pd RadioCoil™ geometry

Iridium

The ^{192}Ir model used was comparable to what has already been published in the literature by the van der Laarse team. The wire is platinum encapsulated with a 0.1 mm core that is ^{192}Ir (ρ = 21.68 g/cm^3) with a 0.1mm sheath of platinum (ρ = 21.45 g/cm^3), yielding a total diameter of 0.3mm. See Figure 3-2.

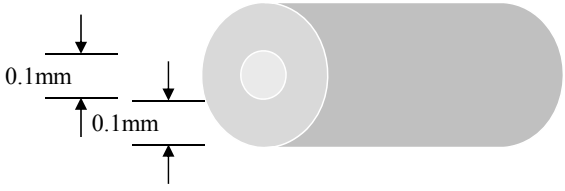

Figure 3-2 ^{192}Ir geometry

3.2 Monte Carlo methods for radiation transport

Monte Carlo simulations were performed on the MCNP5 v5 cluster established by Prof. Rivard at Tufts Medical Center and the photoatomic cross sections based on EPDL97. [16,17,18] The nine good practices for Monte Carlo simulations, as laid out in AAPM TG-43U, were followed.[8] For both radionuclides, source lengths of 0.1 cm through 1.0 cm (step 0.1 cm), 1.5 cm, 2.0 cm, 2.5 cm, and 3.0 cm through 10.0 cm (step 1.0 cm) were calculated. Cylindrical coordinates were used for the sampling geometry, with the *y*-axis defined along the source and the *z*-axis is away from the source. (Figure 2-1) The origin was placed in the center of the source segment. While reviewing the results of previous studies, we questioned whether the sampling space had adequate spatial resolution to accurately estimate the dose distribution. In order to ensure appropriate resolution, the MC spatial resolution was 0.05 cm, although the range varied for the two radionuclides. In both cases, the Monte Carlo simulations calculated kerma using linear track-length estimators or energy deposition (F6 tally) and the Monte Carlo output was in MeV/g/starting particle, which directly correlates to absorbed dose rate, so further calculations were not needed to obtain the absorbed dose rate.[19,20]

An F6 tally track-length estimator for kerma was used for computational efficiency since differences with an absorbed dose estimator (*e.g.*, *F8 MCNP5 tally) would be negligible over the regions examined and for the photon energies of the two radionuclides. In the case of ^{103}Pd, the low-energy source, this assumption was safe since the secondary charged particle (*i.e.*, electron) range was much less than the voxel size. For the high-energy photo-emitter ^{192}Ir, secondary particle/electron range and electron emissions from the thinly encapsulated source needed consideration. Ballester *et al.* reported that collisional kerma and absorbed dose are equivalent within 1% beyond 0.6 mm from an ^{192}Ir source.[21] Additionally, they reported that the electron component to dose exceeded 1% only for $r < 0.2$ cm. To test this further for the source geometries used in this thesis, 1) an F6 collisional kerma tally was compared to a *F8 absorbed dose tally,

both with photon and electron transport, and 2) a *F8 tally with a pure photon-emitting source was compared to the same estimator also having electron source contributions, again with photon and electron transport.[21] These comparisons were performed using the 5.0 cm long ^{192}Ir source. The kerma:dose comparison yielded an average ratio of 1.000±0.001 (k = 1) for 0.2 $\leq r \leq$ 5.0 cm. The electron contribution to total dose for 0.2 $\leq r \leq$ 5.0 cm was less than 0.1% ± 0.05% which was in good agreement with Ballester *et al.* for these distances.[21] It was concluded that the collisional kerma tally (F6) provided an acceptable approximation.

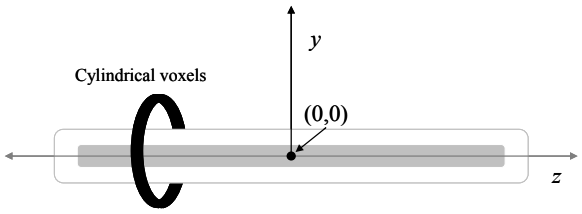

Figure 3-3 Monte Carlo coordinate system. Cylindrical voxels were used to calculate the dose from the source. The voxels were defined by z, the distance along the source and y, the distance away from the source.

Monte Carlo simulations of the ^{103}Pd sources

The ^{103}Pd photon spectrum used was taken from the NuDat database.[22] The dose grid ranged from 0 cm $\leq z \leq$10 cm and 0.2 cm $\leq y \leq$ 12.5 cm, placed in a spherical water phantom with a radius of 15.0 cm (ρ = 0.998 g/cm^3). On average, the statistical uncertainty of the runs was 0.0111. See Table 3-1.

Monte Carlo simulations of the ^{192}Ir sources

The ^{192}Ir photon spectrum used was taken from the NuDat database.[23] The ^{192}Ir β spectrum was not considered as it does not significantly contribute to the dose in this case.[21] The dose grid ranged from 0 cm $\leq z \leq$15 cm and 0.2 cm $\leq y \leq$ 12.5 cm, placed in a

spherical water phantom with a radius of 40.0 cm (ρ = 0.998 g/cm^3). On average, the statistical uncertainty of the runs was 0.0026. See Table 3-1. In the case of both ^{103}Pd and ^{192}Ir, the *y*-axis dose grid began at 0.2 cm so that all the voxels were outside of the source.

Table 3-1 Average statistical uncertainties for each of the Monte Carlo simulations

Length (cm)	^{192}Ir	^{103}Pd
0.1	0.00246	0.01076
0.2	0.00325	0.01426
0.3	0.00248	0.01096
0.4	0.00240	0.01100
0.5	0.00238	0.01134
0.6	0.00314	0.01478
0.7	0.00314	0.01489
0.8	0.00231	0.01503
0.9	0.00232	0.01079
1.0	0.00239	0.01117
1.5	0.00243	0.01116
2.0	0.00250	0.01063
2.5	0.00248	0.01094
3.0	0.00248	0.01081
4.0	0.00247	0.01043
5.0	0.00256	0.00952
6.0	0.00294	0.01257
7.0	0.00291	0.00891
8.0	0.00305	0.00874
9.0	0.00230	0.00799
10.0	0.00217	0.00724

3.3 Preparing Monte Carlo output data for TPS input

In order to use Pinnacle to independently calculate the dose distributions, the data for $g_L(r)$ and $F(r,\theta)$ needed to be derived using the output from the Monte Carlo simulations, which was done using the Tufts technique.[15] The Tufts technique takes the following steps: 1) identify the cylindrical axis of symmetry of the dose distribution, 2) identify the effective length L_{eff}, 3) derive the effective radial dose function, 4) derive the 2D anisotropy function and 5) choose a virtual dose-rate constant at the reference point that reproduces the dose values yielded by the Monte Carlo simulations. The geometry function, $G_L(r,\theta)$, was calculated based on the 2004 AAPM TG-43U1 recommendations,

as explained above, which was then used in conjunction with the MCNP5 output data. Then $g(r)F(r,\theta)$ was calculated as follows:

$$g(r)F(r,\theta) = \frac{\dot{D}(r,\theta)G(r_0,\theta_0)}{G(r,\theta)\dot{D}(r_0,\theta_0)} \tag{11}$$

Setting $F(r,\theta_0) = 1$, the data for $g(r)F(r,\theta_o) = g(r)$. By plotting $g(r)F(r,\theta_o)$, it becomes possible to calculate $g(r)$ for any r, as there is no angular dependence. Excel trendline tools were used to determine formulas that accurately described the various regions of the graph. The behavior of the graph had three distinct regions: $y < 1.0$ cm, $1.0 \text{ cm} \leq y \leq y_{max,}$ and $y > y_{max}$, y_{max} being the farthest tabulated distance on the transverse plane (y-axis) by the Monte Carlo simulations (Figure 3-4 and Figure 3-5). Beyond y_{max}, it was then necessary to extrapolate the data, since the TPS extends beyond the range given by y_{max}. For ^{192}Ir, $y_{max} = 12.5$ cm and for ^{103}Pd, $y_{max} = 10.0$ cm.

In the first region, $y < 1.0$ cm, the dotted line in Figure 3-4 and Figure 3-5, a fourth-order polynomial was used to estimate the shape of the curve. For this region of the graph, there were only 17 data points in each case and the fourth order was visually the best fit for the data, resulting in $R^2 > 0.999$ in all cases. In the region where $1.0 \text{ cm} < y < y_{max}$, the solid line in Figure 3-4 and Figure 3-5, a sixth-order polynomial was used, again because, for both radionuclides, the polynomial fit the graph best and $R^2 > 0.999$ in all cases. The third region had to be treated differently for ^{103}Pd and ^{192}Ir because the drop-off at large distances was greater for ^{103}Pd. The initial plan for characterizing the region defined by $y > y_{max}$ was that a linear extrapolation would be appropriate, given the shape of the curve in the far region. Intending to use the last few data points from the given data, linear approximations were made for both graphs. When this was done for ^{192}Ir, the linear approximation was reasonable and fit the curve nicely. However, for ^{103}Pd, the linear approximation resulted in a $g(r)$ curve that fell below zero, which is not physically possible. As the values at the far distance were so close to zero,

when the values were being tabulated for $r > y_{max}$, a nearest neighbor extrapolation was used setting $g(r > y_{max}) = g(y_{max})$, meaning that when $r > y_{max}$, the value of $g(r)$ at that point was set equal to the value of $g(r = y_{max})$.

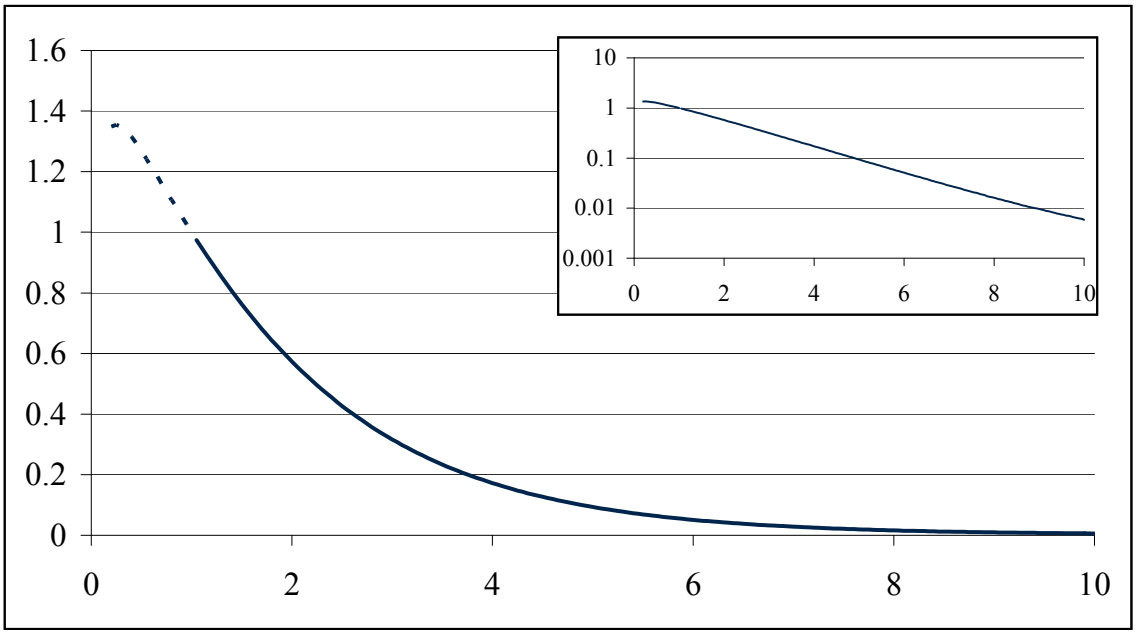

Figure 3-4 $g(r)F(r,\theta_0)$ for ^{103}Pd. The dashed portion is for 0.2 < r < 1.0 cm

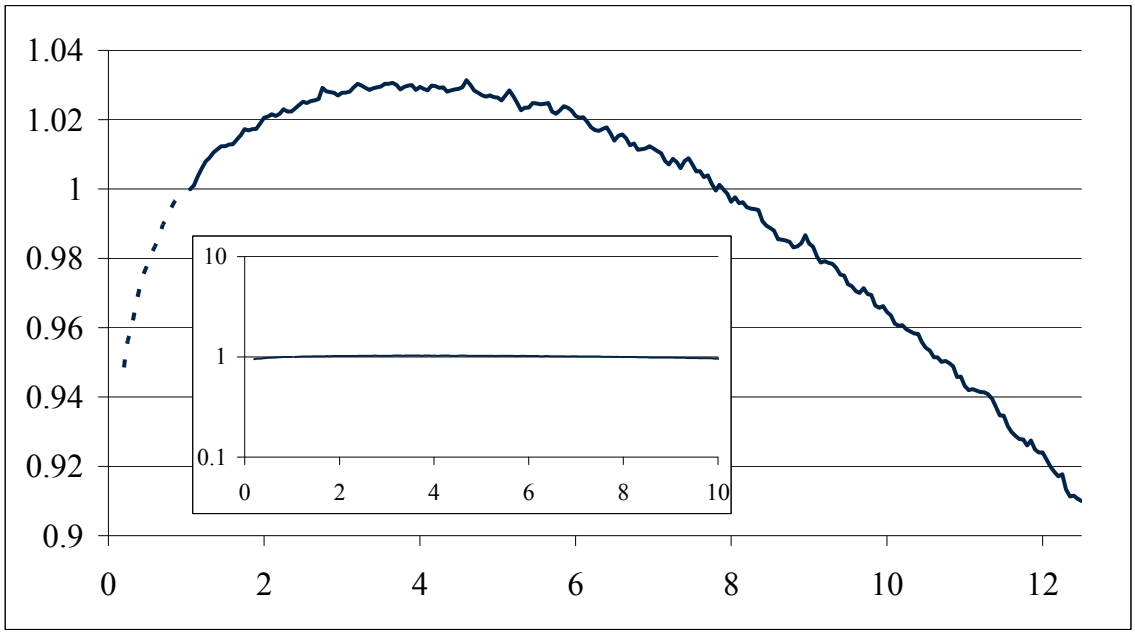

Figure 3-5 $g(r)F(r,\theta_0)$ for ^{192}Ir The dashed portion is for $0.2 < r < 1.0$ cm.

The TPS requires that $g(r)$ and $F(r,\theta)$ be put in terms of $g(y)$ and $F(y,z)$. In order to relate one to the other, simple geometry was used. The following equations explain the relationship.

$$r = \sqrt{y^2 + z^2} \tag{12}$$

$$\theta = \tan^{-1}\left(\frac{y}{z}\right) \tag{13}$$

In this Cartesian coordinate system, it is simple to use the z and y coordinates to determine the correct $g(r)$ for any point, using equation 12. The angular component is taken into account during $G_L(r,\theta)$ calculation. For each length, the values of $g(r)$ were tabulated for a grid that went from 0 to y_{max} in both the z and y direction. Using these tables, $F_{FIT}(r,\theta)$ was calculated in the following way:

$$F_{\mathrm{FIT}}(r,\theta)=\frac{g(r)F(r,\theta)}{g_{\mathrm{FIT}}(r)} \tag{14}$$

It is not necessary to make any correction for the angular component of $F_{\mathrm{FIT}}(r,\theta)$ because, as stated above, this was already satisfied in the calculation of $G_{\mathrm{L}}(r,\theta)$. In the region r<0.2 cm, a nearest neighbor extrapolation was applied in order to complete the table. These values were then tabulated into two tables for each radionuclide length. Once these two tables were derived for each source length, the resolution of both tables was reduced as TPS have limitations in terms of grid size. Further, high-resolution exceeded clinical requirements. Because of these factors, the resolution of the fit of $g(r)$ and $F(r,\theta_{\mathrm{o}})$ were set to 0.2 cm and 0.1 cm respectively. In the case of ^{103}Pd, 0.0 cm $\leq g_{\mathrm{FIT}}(r_0) \leq$ 15.0 cm, step 0.2 cm (51 datapoints) and $F_{\mathrm{FIT}}(r,\theta)$ spanned from 0.0 cm $\leq y \leq$ 10.0 cm, step 0.1 cm, and 0.0 cm $\leq z \leq$ 10.0 cm, step 0.1 cm (10,201 datapoints). This meant that for ^{192}Ir, 0.0 cm $\leq g_{\mathrm{FIT}}(r_0) \leq$ 20.0 cm, step 0.2 cm (101 datapoints) and $F_{\mathrm{FIT}}(r,\theta)$ spanned from 0.0 cm $\leq y \leq$ 15.0 cm, step 0.1 cm, and 0.0 cm $\leq z \leq$ 12.5 cm, step 0.1 cm (19,027 datapoints). In order to speed the process and ensure accuracy, this data was converted into a computer script that automated data input into the Pinnacle TPS.

3.4 Pinnacle TPS

To evaluate the accuracy of the method, it was decided to create a series of 3.0 cm segments and 5.0 cm segments, made up from various lengths in order to complete the comparison with the published literature. 3.0 cm was broken into 1, 3, 4, 5, 6, 10, 15 and 30 segments. 5.0 cm was broken into 2, 5, 10, 25 and 50 segments. Table 3-2 details the 3.0 cm lengths used for each trial and Table 3-3 details the 5.0 cm lengths used.

Table 3-2 Segment lengths used in Pinnacle to approximate a 3.0 cm source length.

Segment length (cm)	Number of Segments	Source Strength (U)
3.0	1	1.0000
1.5	2	0.5000
1.0	3	0.3333
0.8/0.7	4 (2 each)	0.2667, 0.2333
0.6	5	0.2000
0.5/1.0	4 (2 each)	0.1667, 0.3333
0.5	6	0.1667
0.3	10	0.1000
0.2	15	0.0667
0.1	30	0.0333

Table 3-3 Segment lengths used in Pinnacle to approximate a 5.0 cm source length

Segment length (cm)	Number of Segments	Source Strength (U)
5.0	1	1.000
2.5	2	0.500
1.0	5	0.200
0.5	10	0.100
0.2	25	0.040
0.1	50	0.020

Within Pinnacle TPS, the calculation space (Table 3-4) was chosen to be large enough to ensure an accurate depiction of the dose distribution. The dose grid was limited by the TPS and was set to 0.2 cm. In clinical practice, 0.2 cm accuracy for a brachytherapy source placement is adequate.

Table 3-4 Description of the calculation space within Pinnacle where dose calculations were performed. The X axis described the plane that the source was placed in, the Y axis is along the source, and the Z axis is away from the source.

	X	Y	Z
Calculation Space			
Voxel Size (cm)	0.25	0.25	0.25
Data Points	208	208	208
Spatial Extent (cm)	52.0	52.0	52.0
Dose Grid			
Voxel Size (cm)	0.2	0.2	0.2
Data Points	3	201	201
Spatial Extent (cm)	0.6	40.2	40.2

This calculated space was duplicated for all of the line source configurations in Table 3-2 and Table 3-3. Each configuration was then built within the TPS, calculated, and the data exported.

3.5 IBA Dosimetry OmniPro-I'mRT

In order to compare the results of the 3.0 cm line segments with the various configurations, OmniPro-I'mRT by IBA Dosimetry was used. There were a number of reasons that this type of analysis was performed. Fluence maps, depicting dose distributions, can be exported from Pinnacle and directly imported into OmniPro-I'mRT without any formatting. Extra steps to perform the comparisons within Excel would have been required. OmniPro-I'mRT can perform all of the same calculations that Excel can handle without programming, as well as allowing visual depictions of the dose distributions comparisons.

The Gamma method [24] was employed to compare the dose of the L = 3.0 cm or L = 5.0 cm source lengths to all configurations from Table 3-2 and Table 3-3, respectively, to the dose at the same point. This permitted a threshold both in terms of distance and dose. The calculation that the software performs is defined by the following:

$$\gamma(r_m) = \min\{\Gamma(r_m, r_c)\}\forall\{r_c\} \text{ where} \quad (15)$$

$$\Gamma(r_m, r_c) = \sqrt{\frac{r^2(r_m, r_c)}{\Delta d_M^2} + \frac{\delta^2(r_m, r_c)}{\Delta D_M^2}},$$

$$r(r_m, r_c) = |r_c - r_m| \text{ and}$$

$$\delta(r_m, r_c) = D_c r_c - D_m r_m$$

r_m is the position of a single measurement point, r_c is the spatial location of the calculated distribution relative to the measurement point, Δd_M is the passing criteria for isodose distance, ΔD_M is the passing criteria for dose, $D_c(r_c)$ is the calculated dose in r_c and $D_m(r_m)$ is the measured dose in r_m. Two comparisons were done. The more strict comparison defined Δd_M as 0.1 cm and ΔD_M was chosen to be 1%. Additionally, ΔD_M was chosen to be 2% (Δd_M remained the same) for comparison.

CHAPTER 4

RESULTS AND DISCUSSION

4.1 Excel comparison

As a quick check of principle, the superposition principle was applied within Excel, taking the MC output files and directly using them to sum to various lengths. The same comparisons were made in Excel as were made in OmniPro I'mRT, as detailed in Table 3-2 and Table 3-3. In all cases, the superposition principle worked as expected. Along the transverse plane, the average ratio of the superposition to the solid source was 1.007 for ^{103}Pd and 0.999 for ^{192}Ir. Overall, the average ratio over the whole grid was 1.051 for ^{103}Pd and 1.009 for ^{192}Ir. For both ^{103}Pd and ^{192}Ir, the instances where the sources were made up of variable lengths (i.e. two 0.5 cm lengths and two 1.0 cm lengths) produced the worst results, particularly along the transverse plane. One reason for this could be that the segments were treated as if they had the same activity. However, weighting of the segments would have to reflect the relative mass that each length comprises. Results improved as the number of lengths used were reduced, with the best results stemming from the long source (3.0 cm or 5.0 cm) being divided into two pieces (1.5 cm or 2.5 cm). This was expected because the approximation of attenuation along the length of the source is more accurate for a longer segmentation (or fewer segments).

Table 4-1 The ratio of the segmented source to the full source in Excel using the raw ^{103}Pd Monte Carlo data.

			Excel Superposition ratios			
Total Length (cm)	Length of Segments	Number of Segments	Average	Max	Min	Transverse plane average
3	1.5 cm	2	1.009	1.212	0.901	1.001
3	1.0 cm	3	0.999	1.188	0.681	1.008
3	2x0.5 cm + 2x1.0 cm	4	1.056	1.479	0.373	0.966
3	2x0.8 cm + 2x0.7 cm	4	1.025	1.234	0.735	1.002
3	0.6 cm	5	1.018	1.218	0.635	1.015
3	0.5 cm	6	1.026	1.251	0.561	1.016
3	0.3 cm	10	1.088	1.328	0.956	1.031
3	0.2 cm	15	1.130	1.424	0.969	1.049
3	0.1 cm	30	1.011	1.525	0.685	0.763
5	2.5 cm	2	1.004	1.150	0.933	1.000
5	1.0 cm	5	1.019	1.168	0.957	1.011
5	0.5 cm	10	1.043	1.272	0.847	1.021
5	0.2 cm	25	1.110	1.440	0.969	1.030
5	0.1 cm	50	1.210	1.695	1.022	1.113

Table 4-2 The ratio of the segmented source to the full source in Excel using the raw ^{192}Ir Monte Carlo data.

			Excel Superposition ratios			
Total Length	Length of Segments	Number of Segments	Average	Max	Min	Transverse plane average
3	1.5 cm	2	1.002	1.068	0.983	1.000
3	1.0 cm	3	1.003	1.115	0.989	1.000
3	2x0.5 cm + 2x1.0 cm	4	1.009	1.380	0.781	0.979
3	2x0.8 cm + 2x0.7 cm	4	1.003	1.166	0.776	0.995
3	0.6 cm	5	1.006	1.199	0.992	1.001
3	0.5 cm	6	1.007	1.242	0.853	1.000
3	0.3 cm	10	1.013	1.376	0.994	1.000
3	0.2 cm	15	1.019	1.511	0.995	1.001
3	0.1 cm	30	1.033	1.701	0.997	1.002
5	2.5 cm	2	1.001	1.069	0.968	1.000
5	1.0 cm	5	1.003	1.121	0.991	1.001
5	0.5 cm	10	1.007	1.245	0.994	1.001
5	0.2 cm	25	1.010	1.522	0.959	0.968
5	0.1 cm	50	1.022	1.709	0.998	1.004

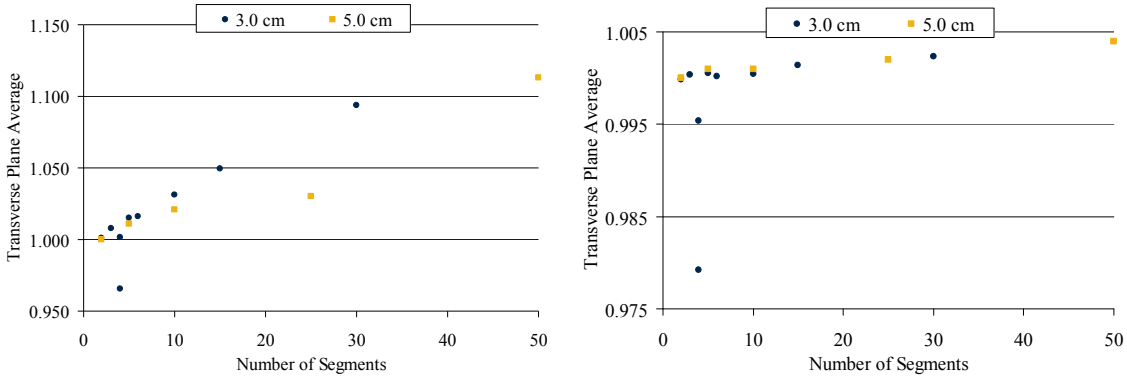

(a) (b)

Figure 4-1 Plot of the number of line segments versus the transverse plane average dose for (a) ^{103}Pd and (b) ^{192}Ir.

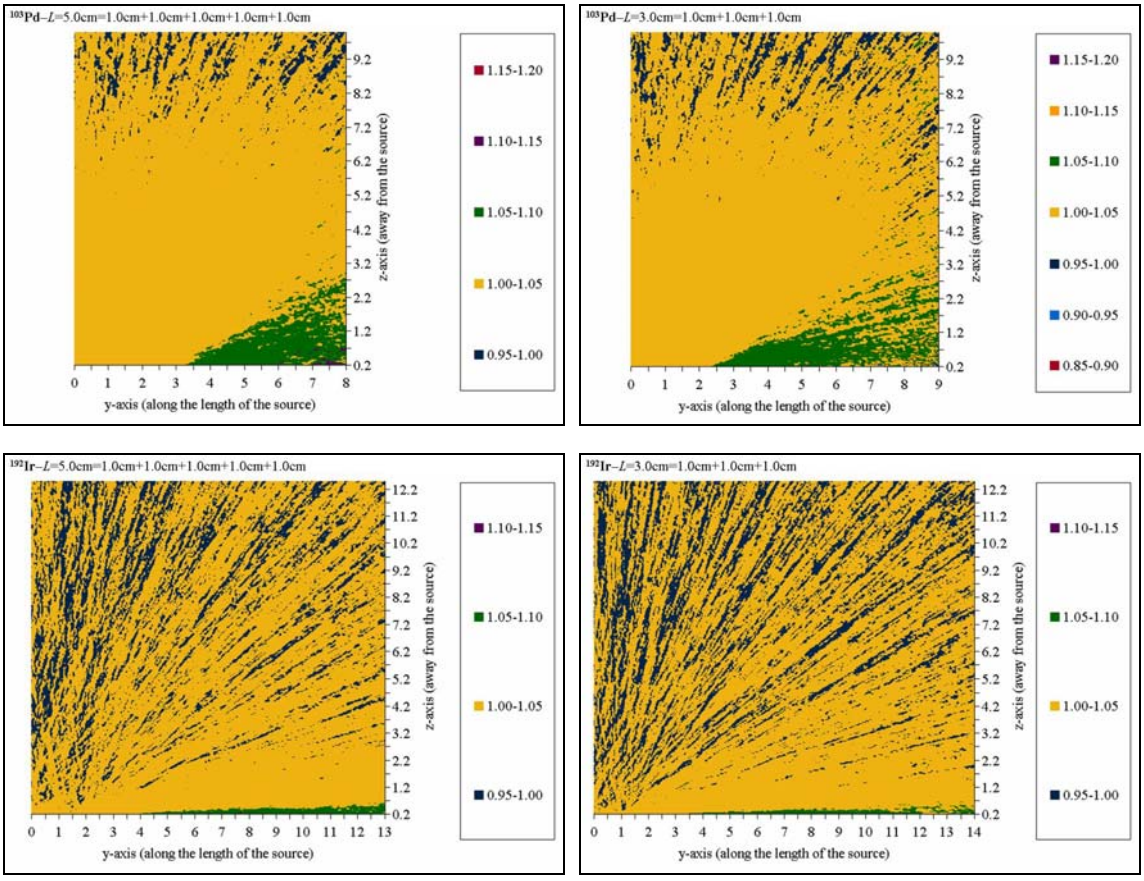

(a) (b)

Figure 4-2 Sample plot of the dose ratio of segmented source to the intact source for (a) 5.0 cm = 1.0cm+1.0cm+1.0cm+1.0cm+1.0cm and (b) 3.0 cm = 1.0cm+1.0cm+1.0cm. For both, ^{103}Pd is on the top and ^{192}Ir is on the bottom.

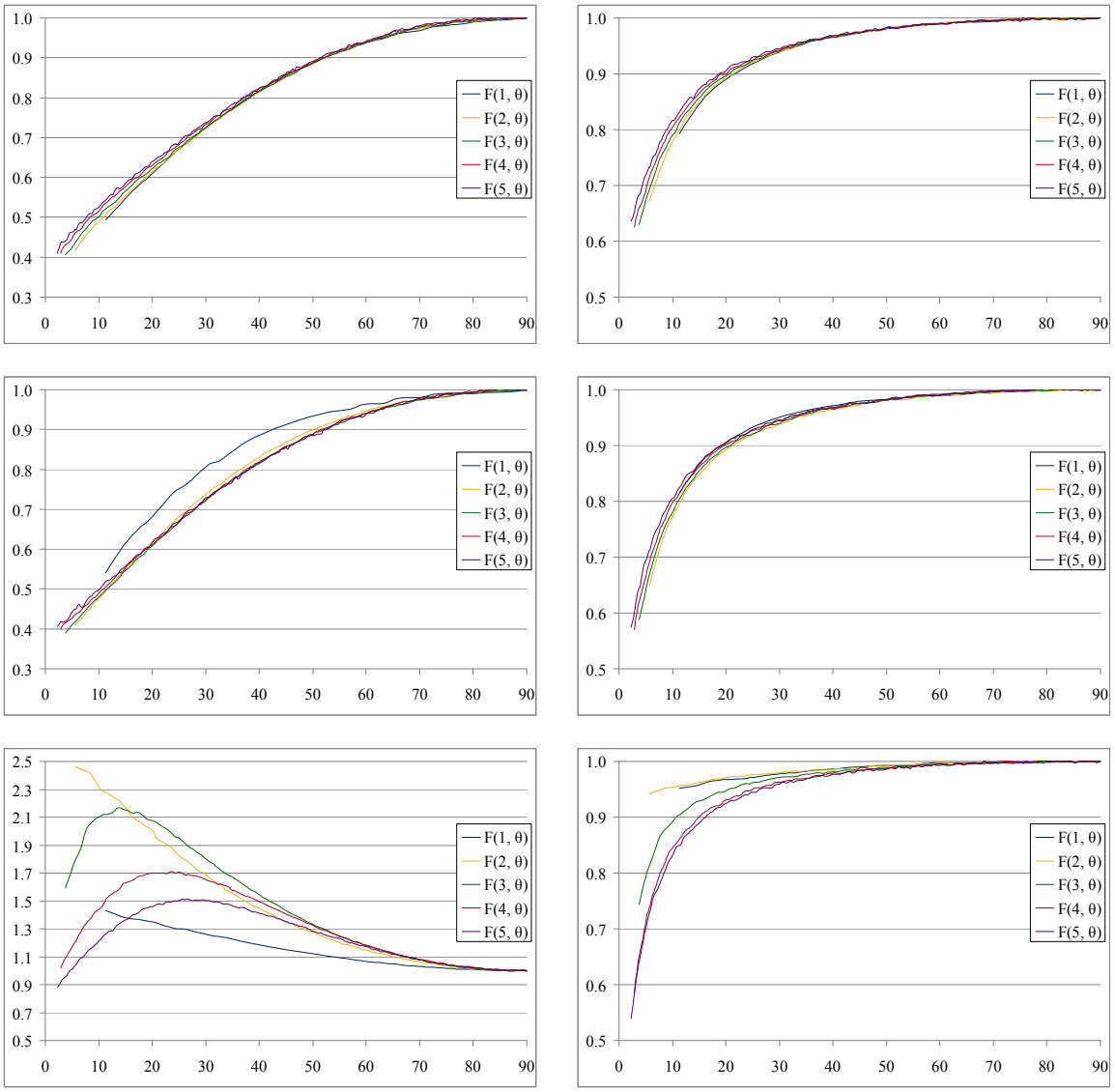

Figure 4-3 Plot of $F(r,\theta)$ for a variety of r values. ^{103}Pd is on the left and ^{192}Ir is on the right. The topmost pair is for L = 0.5 cm, the middle pair is for L = 1.0 cm and the bottom pair is for L = 5.0 cm. As expected, $F(r,\theta)$ for all values approaches 1 as θ approaches 90º. This is expected as this is the reference point (r=1.0 cm, θ = 90º) and was chosen to be 1. Note that the $F(r,\theta)$ values for L = 0.5 cm and L = 1.0 cm are comparable. This was previously reported in the literature, however had not been quantified.

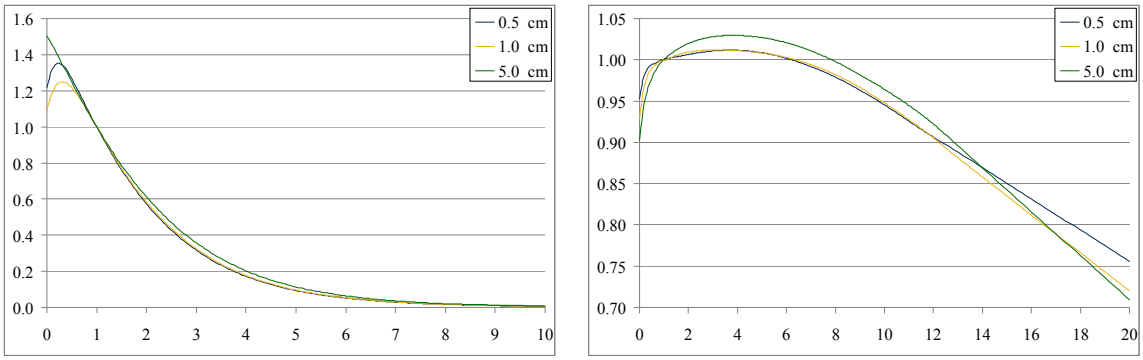

Figure 4-4 $g(r)$ for L = 0.5 cm, L = 1.0 cm and L = 5.0 cm. ^{103}Pd is on the left and ^{192}Ir is on the right.

4.2 Pinnacle results

A visual inspection of the Pinnacle results indicated agreement with the Excel results. Isodose lines that intersected the transverse plane remained constant over the range of line segments examined. However, the isodose lines that intersected the source long axis became less accurate as the number of segments increased.

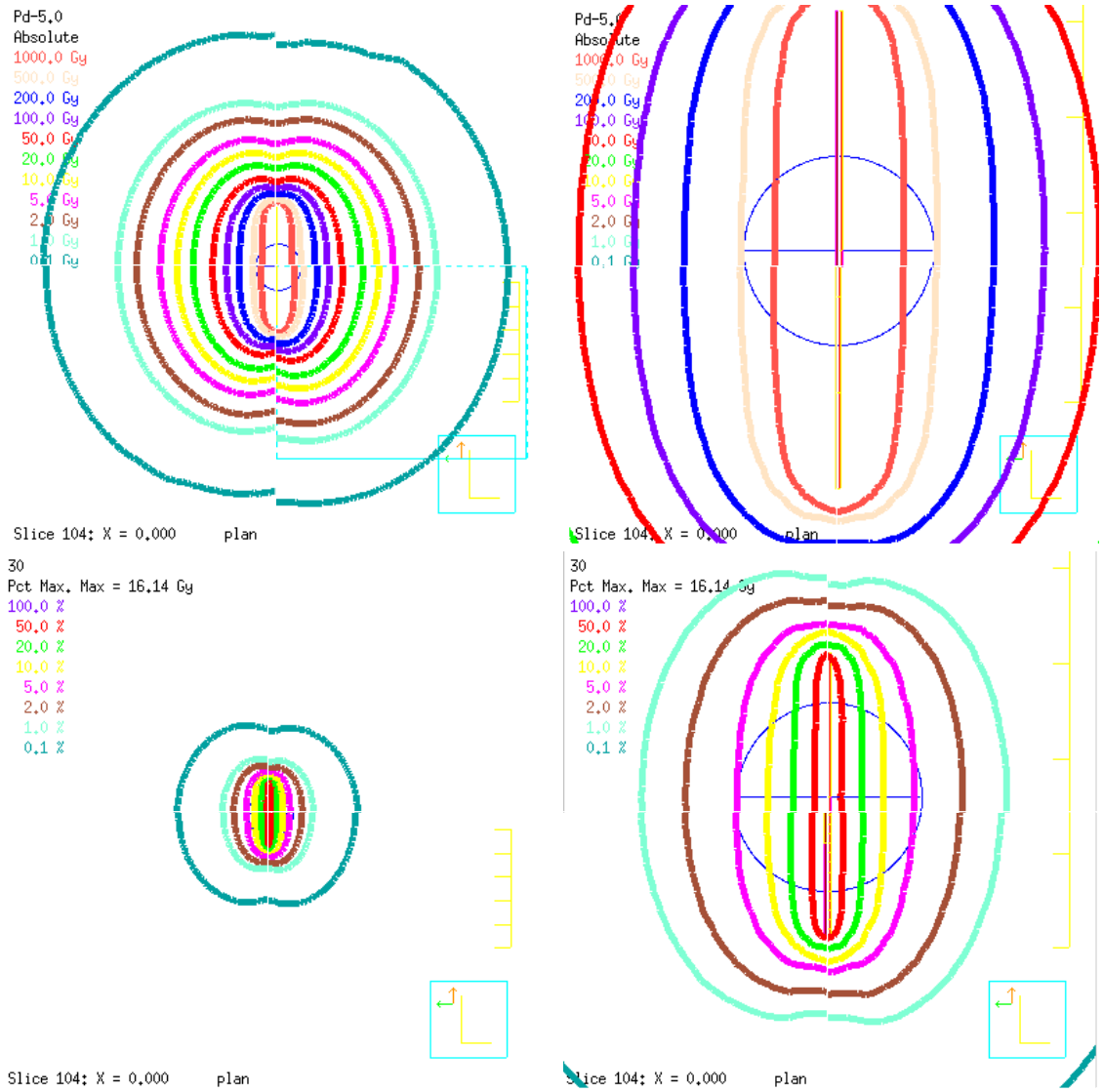

Figure 4-5 Isodose maps for ^{103}Pd. Each image contains four quadrants. The top left hand quadrant is the whole source in one segment. The top right hand quadrant is the source broken into two segments. The bottom left hand quadrant is the length broken into 1.0 cm segments, and the bottom right hand quadrant is the source broken into 0.1 cm lengths. The column on the left is a wide perspective as shown by the yellow ruler/scale, while the right hand column zooms in to a 3.0 cm width. The blue circle is 1.0 cm in radius. The 5.0 cm lengths are on the top row and the bottom row is the 3.0 cm lengths. In all cases, the plane that bisects the source in the middle produced good results, while the results from the source long-axis deteriorated as the number of segments increased.

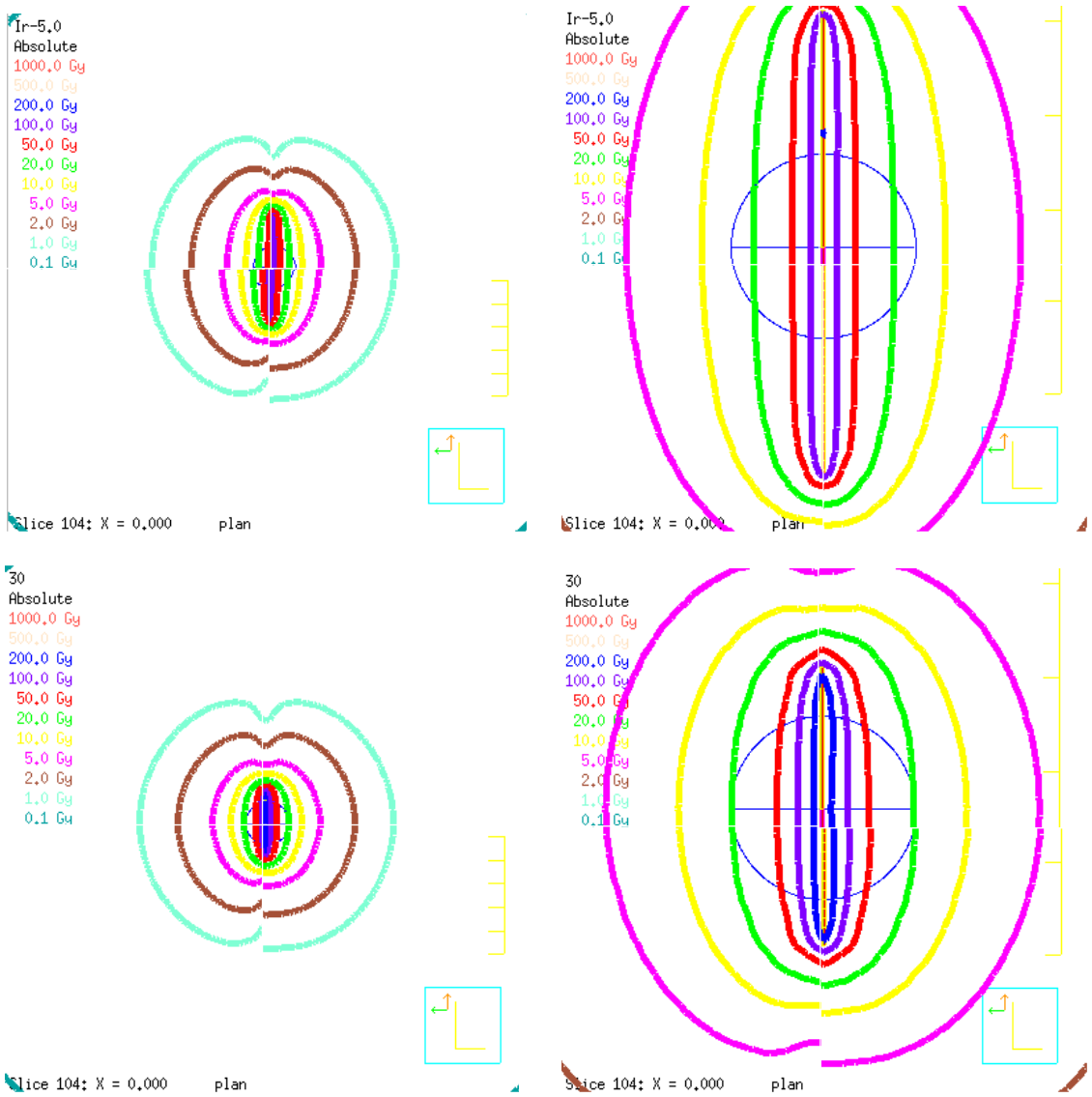

Figure 4-6 Similar approach to those in Figure 4-5, except for ^{192}Ir. The results were also similar in that the comparison along the transverse plane produced good results while the results on the long axis diminished as the number of segments increased.

4.3 IBA Dosimetry

Comparisons were made with ΔD_m set to both a 1% tolerance and a 2% tolerance within the IBA Dosimetry OmniPro I'mRT, with Δd_m = 2.0 mm. In comparing the 3.0 cm length of ^{103}Pd, three 1.0 cm segments produced the best comparison with 99.2% of the pixels passing ΔD_m = 2%. For the 3.0 cm length of ^{192}Ir, the best results were for the

model comprised of three 1.0 cm segments, with 100.0% of the pixels passing for ΔD_m = 2%. Comparing these results to the LSS results of Meigooni *et. al*, showed a marked improvement in methodology. Their results averaged a 4% dose difference (with fewer positions across the dose grid reported), with a maximum difference of 14% for ^{103}Pd. They did not simulate ^{192}Ir so direct comparison is not possible. However, the results that are reported in this work demonstrate that the Tufts technique achieves a pass rate that is well within acceptable margins of error.[8]

Comparing our results to the TLS method produced similar observations. The OmniPro-I'mRT Gamma comparison determined that, for the ^{103}Pd 5.0 cm length, two 2.5 cm segments yield the best results, with 98.7% of the pixels passing with ΔD_m = 2%. ^{192}Ir had the best comparison for five 1.0 cm segments, with 99.7% passing with ΔD_m = 2%. This is an improvement over the TLS method, which had discrepancies of up to 5.6% along the transverse plane. Additionally, the TLS method is not clinically implementable, while the Tufts technique is, which means that the results are not only numerically superior but also practicable.

Table 4-3 Percent of pixels passing a gamma test within OmniPro-I'mRT for both ^{103}Pd and ^{192}Ir.

	Pd		Ir	
3.0 cm	**1 %, 2 mm**	**2 %, 2 mm**	**1 %, 2 mm**	**2 %, 2 mm**
(n x mm)	%	%	%	%
2 x 15.0	98.2	99.1	99.1	99.5
3 x 10.0	98.5	99.2	99.8	100.0
8.0+7.0+7.0+8.0	98.6	99.2	98.2	99.1
5 x 6.0	97.7	98.4	99.5	99.8
5.0 + 10.0 + 10.0 + 5.0	98.2	99.2	99.5	99.8
6 x 5.0	97.8	99.2	99.2	99.8
10 x 3.0	97.1	98.5	99.3	99.7
15 x 2.0	97.0	98.2	98.9	99.5
30 x 1.0	98.1	98.9	98.8	99.4
5.0 cm				
(n x mm)				
2 x 25.0	97.5	98.7	98.3	99.1
5 x 10.0	96.5	97.9	98.8	99.7
10 x 5.0	94.8	98.0	98.1	99.0
25 x 2.0	94.3	96.0	97.8	98.5
50 x 1.0	95.3	97.6	97.5	98.2

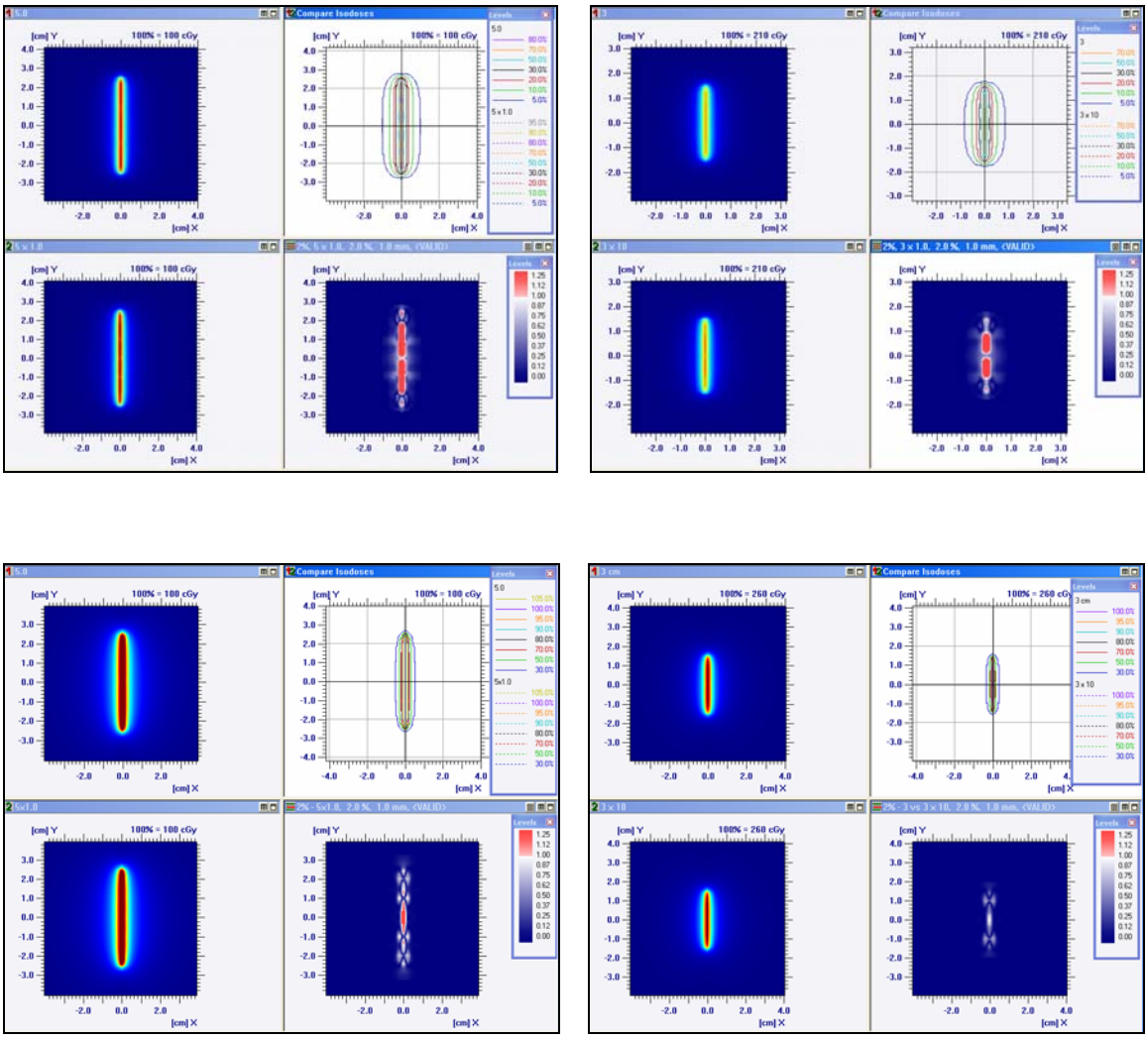

Figure 4-7 Gamma comparison of the 5.0 cm length to the 5.0 cm length that was made up of five 1.0 cm segments (left) and the 3.0 cm length to the three 1.0 cm segments (right). ^{103}Pd is on the top and ^{192}Ir is on the bottom.

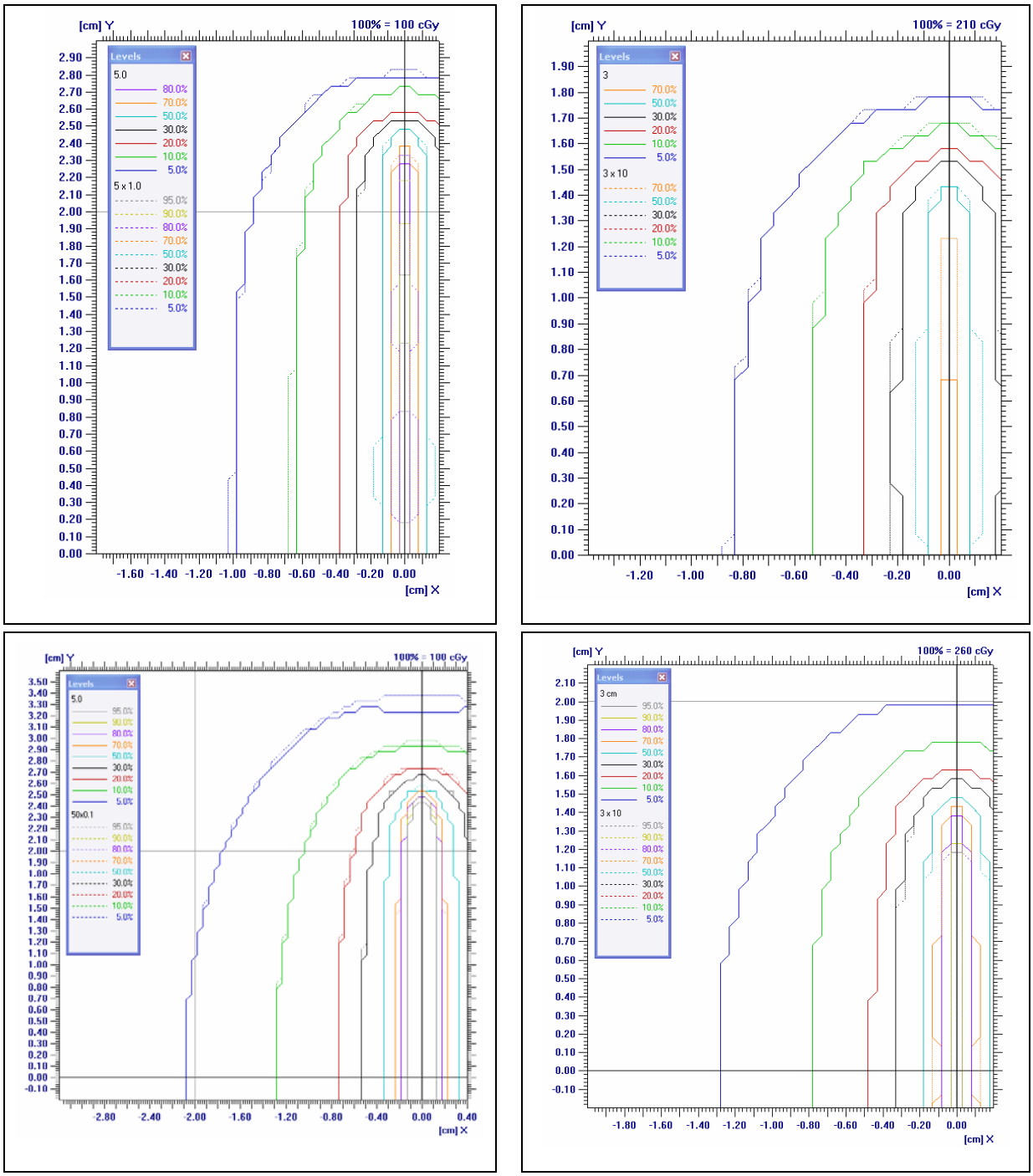

Figure 4-8 Comparison of the isodose lines of the 5.0 cm length to the five 1.0 cm segments (left) and of the 3.0 cm length to the three 1.0 cm lengths (right). ^{103}Pd is on the top and ^{192}Ir is on the bottom. The agreement is seen to be worst in the areas at the end of the source as well as very close to the source. However, overall agreement is quite good.

CHAPTER 5

CLOSING

As expected, the superposition principle for brachytherapy dose calculation worked upon dividing the elongated sources into smaller segments. Dosimetric differences were, on average, less than 1% in the majority of locations in the vicinity of each source. It is clear that the anisotropy of the elongated source needs to be one of the most important criteria in developing a series of suggestions for treatment planning.

Techniques were developed that can be used clinically, making dosimetric calculations of elongated sources an easy task that can be undertaken to ensure patient safety. The Tufts technique permitted derivation of the anisotropy and radial dose functions on a clinical TPS.

IBA dosimetry tools, which were developed for IMRT QA, were used in a novel way to analyze brachytherapy isodose curves. It is possible that this approach could be used to perform QA on patients who are implanted with brachytherapy sources, to compare the desired/ideal seed configuration to the actual outcome. A CT scan can be performed before the surgery, and the medical physicist and physician can work to decide the best placement of the source. After the surgery, another CT can be acquired and the real source placement can be calculated in Pinnacle. These two datasets can then be compared using the OmniPro-I'mRT software.

The next step of this work is to move beyond straight-elongated sources and extend the analysis to curved sources and then curvilinear sources. In the practice of brachytherapy, it is necessary to have brachytherapy sources physically conform to the patient's anatomy. One important question to answer is, "What is the correlation between the radius of a curved portion of a source and the straight-length approximation?" If the arc is approximated with a length that it too short, there is not enough attenuation and the

dose is too high. However, if the length is too long, it no longer conforms to the shape of the source and the self-attenuation becomes too great.

Additionally, tables should be developed, using Monte Carlo techniques, for a variety of sources that can then be used as a standard set of segments to be used in treatment planning for elongated brachytherapy cases. From this research, it seems that longer segments will be more useful than shorter segments (i.e. <0.5 cm), since shorter segments are problematic in terms of accounting for dose anisotropy. These tables can then be used as standards within the medical community.

REFERENCES

[1] H. Danlos and P. Bloch, "Note sur le traitement du lupus érythèmateux par des applications de radium," Ann. Dermatol. Syphil. **2**, 986–988 (1901).

[2] R. Abbé, "Notes on the physiologic and therapeutic action of radium," Wash. Med. Ann. 2, 363–377 (1904).

[3] A. G. Bell, "The uses of radium," Am. Med. 6, 261 (1903).

[4] S. B. Awan, A. S. Meigooni, R. Mokhberiosgouei, and M. Hussain, "Evaluation of TG-43 recommended 2D-anisotropy function for elongated brachytherapy sources," Med. Phys. 33, 4271–4279 (2006).

[5] B. R. Thomadsen, J. F. Williamson, M. J. Rivard, and A. S. Meigooni, "Anniversary Paper: Past and current issues, and trends in brachytherapy physics," Med. Phys. 35, 4708–4723 (2008).

[6] R. J. Shalek and M. A. Stovall, "Dosimetry in implant therapy," in *Radiation Dosimetry vol 3,* edited by F. H. Attix and E. Tochlin (Academic, New York, 1969), pp. 776–798.

[7] R. Nath, L. L. Anderson, G. Luxton, K. A. Weaver, J. F. Williamson, and A. S. Meigooni, "Dosimetry of interstitial brachytherapy sources: Recommendations of the AAPM Radiation Therapy Committee Task Group No. 43. American Association of Physicists in Medicine," Med. Phys. 22, 209–234 (1995).

[8] M. J. Rivard, B. M. Coursey, L. A. DeWerd, W. F. Hanson, M. S. Huq, G. S. Ibbott, M. G. Mitch, R. Nath, and J. F. Williamson, "Update of AAPM Task Group No. 43 Report: A revised AAPM protocol for brachytherapy dose calculations," Med. Phys. 31, 633–674 (2004).

[9] M. J. Rivard, W. M. Butler, L. A. DeWerd, M. S. Huq, G. S. Ibbott, A. S. Meigooni, C. S. Melhus, M. G. Mitch, R. Nath, and J. F. Williamson, "Supplement to the 2004 update of the AAPM Task Group No. 43 Report," Med. Phys. 34, 2187–2205 (2007).

[10] P. Karaiskos, P. Papagiannis, A. Angelopoulos, L. Sakelliou, D. Baltas, P. Sandilos, and L. Vlachos, " Dosimetry of ^{192}Ir wires for LDR interstitial brachytherapy following the AAPM TG-43 dosimetric formalism," Med. Phys. 28, 156–166 (2001).

[11] A. S. Meigooni, S. B. Awan, V. Rachabatthula, and R. A. Koona, "Treatment-planning considerations for prostate implants with the new linear RadioCoil™ ^{103}Pd brachytherapy source, " J. Appl. Clin. Med. Phys. 6, 23–36 (2005).

[12] R. van der Laarse, D. Granero, J. Perez-Calatayud, Ali. S. Meigooni, and F. Ballester, "Dosimetric characterization of Ir-192 LDR elongated sources," Med. Phys. 35, 1154–1161 (2008).

[13] P. Karaiskos, A. Angelopoulos, P. Baras, H. Rozaki-Mavrouli, P. Sandilos, and L. Sakelliou, " Dose rate calculations around brachytherapy sources using a Sievert integration model," Phys. Med. Biol. 45, 383–397 (2000).

[14] A. S. Meigooni, H. Zhang, J. R. Clark, V. Rachabatthula, and R. A. Koona, "Dosimetric characteristics of the new RadioCoil™ ^{103}Pd wire line source for use in permanent brachytherapy implants," Med. Phys. 31, 3095–3105 (2004).

[15] M. J. Rivard, C. S. Melhus, D. Granero, J. Perez-Calatayud, and F. Ballester, "An approach to using conventional brachytherapy software for clinical treatment planning of complex, Monte Carlo-based brachytherapy dose distributions," Med. Phys. 36, 1968–1975 (2009).

[16] X-5 Monte Carlo Team, "MCNP: A general Monte Carlo *N*-particle transport code," Version 5, Los Alamos National Laboratory, Los Alamos, NM, 2003.

[17] M. White, " Photoatomic data library MCPLIB04: A new photoatomic library based on data from ENDF/B-VI release 8," Los Alamos National Laboratory Memorandum No. LAUR-03-1019, 2003.

[18] D. E. Cullen, J. H. Hubbell, and L. Kissel, "EPDL97: The Evaluated Photon Data Library, '97 Version," Lawrence Livermore National Laboratory Report No. UCRL-50400 (19 September 1997).

[19] M. J. Rivard, D. Granero, J. Perez-Calatayud, and F. Ballester, "Influence of photon energy spectra from brachytherapy sources on Monte Carlo simulations of kerma and dose rates in water and air," Med. Phys. 37, 869–876 (2010).

[20] C. S. Melhus and M. J. Rivard, "Approaches to calculating AAPM TG-43 brachytherapy dosimetry parameters for ^{137}Cs, ^{125}I, ^{192}Ir, ^{103}Pd, and ^{169}Yb sources," Med. Phys. 33, 1729–1737 (2006).

[21] F. Ballester, D. Granero, J. Perez-Calatayud, C. S. Melhus, and M. J. Rivard, "Evaluation of high-energy brachytherapy source electronic disequilibrium and dose from emitted electrons," Med. Phys. 36, 4250–4256 (2009).

[22] NUDAT 2.4, National Nuclear Data Center, Brookhaven National Laboratory, http://www.nndc.bnl.gov/nudat2/decaysearchdirect.jsp?nuc=103Pd, (last accessed 8 March 2010).

[23] NUDAT 2.4, National Nuclear Data Center, Brookhaven National Laboratory, http://www.nndc.bnl.gov/nudat2/decaysearchdirect.jsp?nuc=192Ir, (last accessed 8 March 2010).

[24] M. Stock, B. Kroupa, and D. Georg, "Interpretation and evaluation of the gamma index and the gamma index angle for the verification of IMRT hybrid plans," Phys. Med. Biol. 50, 399–411 (2005).